NANOPHOTONICS

Continuous-wave frequency upconversion with a molecular optomechanical nanocavity

Wen Chen[1], Philippe Roelli[1]†, Huatian Hu[2], Sachin Verlekar[1], Sakthi Priya Amirtharaj[1], Angela I. Barreda[3], Tobias J. Kippenberg[1], Miroslavna Kovylina[4], Ewold Verhagen[5], Alejandro Martínez[4], Christophe Galland[1]*

Coherent upconversion of terahertz and mid-infrared signals into visible light opens new horizons for spectroscopy, imaging, and sensing but represents a challenge for conventional nonlinear optics. Here, we used a plasmonic nanocavity hosting a few hundred molecules to demonstrate optomechanical transduction of submicrowatt continuous-wave signals from the mid-infrared (32 terahertz) onto the visible domain at ambient conditions. The incoming field resonantly drives a collective molecular vibration, which imprints a coherent modulation on a visible pump laser and results in upconverted Raman sidebands with subnatural linewidth. Our dual-band nanocavity offers an estimated 13 orders of magnitude enhancement in upconversion efficiency per molecule. Our results demonstrate that molecular cavity optomechanics is a flexible paradigm for frequency conversion leveraging tailorable molecular and plasmonic properties.

Control and analysis of electromagnetic signals spanning the full spectrum from radio waves to x-rays governs technological progress in areas ranging from information processing, telecommunication networks, material characterization, spectroscopy, and imaging to remote sensing. The mid- and far-infrared (IR) frequency range, from a few to 100 THz, finds applications such as in homeland security, molecular analysis of gases, chemicals and biological tissues (*1*), thermal imaging and nondestructive material inspection (*2*), and astronomical surveys (*3*). However, IR detection technologies (*4*) do not rival with visible and near-infrared (VIS/NIR) detectors in terms of sensitivity, cost-effectiveness, and integration, motivating new approaches to perform IR spectroscopy with VIS/NIR detectors. Such methods include nonlinear interferometers (*5*, *6*) and coherent frequency upconversion (*7*, *8*), which is compatible with quantum technologies (*9*, *10*). Coherent upconversion of IR signals can be accomplished with bulk nonlinear optics using three-wave mixing processes, but delicate phase matching and propagation in centimeter-long crystals are needed to reach high efficiencies (*11*, *12*). Three-wave mixing may also occur at nanoscale interfaces and is used to probe the properties and dynamics of molecular layers with ultrafast nonlinear spectroscopy (*13*, *14*); however, such techniques require substantial peak powers only accessible with femto- or picosecond pulses.

Optomechanical cavities have recently emerged as promising candidates to realize quantum coherent frequency conversion (*9*, *10*, *15*). In a possible implementation, the signal of interest resonantly drives a mechanical oscillator, itself parametrically coupled to a laser-driven optical cavity, which results in modulation sidebands at the sum and difference frequencies (called anti-Stokes and Stokes sidebands, respectively). This approach offers a number of advantages, such as the resonant enhancement of nonlinear response at the mechanical frequency and

[1]Institute of Physics, Ecole Polytechnique Fédérale de Lausanne (EPFL), CH-1015 Lausanne, Switzerland. [2]Hubei Key Laboratory of Optical Information and Pattern Recognition, Wuhan Institute of Technology, Wuhan 430205, China. [3]Institute of Applied Physics, Abbe Center of Photonics, Friedrich Schiller University Jena, 07745 Jena, Germany. [4]Nanophotonics Technology Center, Universitat Politècnica de València, 46022 Valencia, Spain. [5]Center for Nanophotonics, AMOLF, 1098 XG Amsterdam, Netherlands.
*Corresponding author. Email: chris.galland@epfl.ch
†Present address: Nano-optics Group, CIC nanoGUNE BRTA, E-20018 Donostia, San Sebastián, Spain.

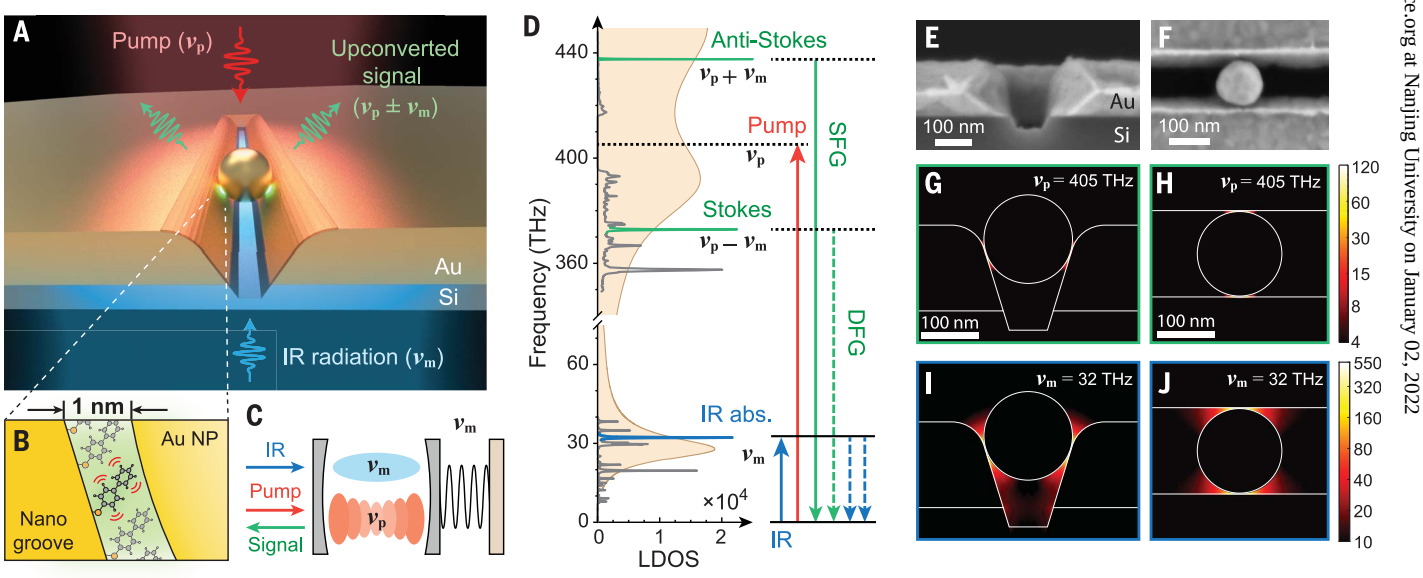

Fig. 1. Molecular optomechanical upconversion concept. (**A**) Illustration of a nanoparticle-in-groove cavity confining IR (frequency ν_m) and VIS (frequency ν_p) fields into a ~1-nm-thick BPhT molecular layer (**B**) Au NP, gold nanoparticle (~150 nm diameter). (**C**) The molecular vibration resonantly couples to the IR field and parametrically couples (through the Raman polarizability) to the VIS field, realizing an optomechanical cavity. (**D**) Vibrational levels and transitions involved in upconversion. LDOS, computed radiative local density of state inside the nanocavity. The measured Raman scattering and simulated molecular IR absorption (compare supplementary materials, section 1.5) are overlaid. SFG/DFG, sum frequency generation/difference frequency generation. (**E** and **F**) Cross-sectional scanning electron microscope (SEM) image of a fabricated nanogroove (E) and top view of a nanoparticle-in-groove (F). (**G** to **J**) Simulated electromagnetic field enhancement factors for incident plane waves at ν_p = 405 THz [740 nm; (G) and (H)] and ν_m = 32 THz [9.3 μm; (I) and (J)], both polarized orthogonally to the groove.

the parametric enhancement of conversion efficiency with intracavity pump power. It is highly versatile and has been demonstrated with mechanical resonance frequencies ranging from kilohertz (*16*) to gigahertz (*17*–*21*). In a different approach, modulations on terahertz waves have been read out optically through a megahertz-frequency mechanical resonator (*22*). Molecular oscillators constitute a new frontier in cavity optomechanics (*23*, *24*) because they enable multi-terahertz resonant frequencies and room temperature quantum coherent operation (*25*). Moreover, they can be coupled to plasmonic nanocavities with deep-subwavelength mode volumes, thereby enabling optomechanical coupling rates in excess of 1 THz (*26*). Although plasmonic gap modes have been demonstrated to substantially enhance other nonlinear effects (*27*–*29*), frequency conversion devices based on molecular cavity optomechanics have yet to be demonstrated.

Here, we experimentally demonstrate the upconversion of continuous wave IR signal at ~32 THz (9.3 μm wavelength) into the visible domain using a subwavelength molecular optomechanical cavity at ambient conditions. Our upconversion scheme operates with microwatt-level continuous wave signal and pump beams and allows high-resolution spectroscopy of the IR signal because of the coherent nature of optomechanical transduction. This regime of operation is achieved by coupling a molecular monolayer to a doubly resonant plasmonic gap nanocavity, which supports deep-subwavelength mode volumes and simulated field enhancement factors in excess of 500 and 100 at IR and VIS frequencies, respectively, from which an overall enhancement of upconversion efficiency per molecule by >13 orders of magnitude compared with free space is predicted and experimentally validated.

A molecular optomechanical platform for upconversion was proposed in (*23*) and its theoretical performance was analyzed in (*8*), showing the feasibility of single-photon sensitivity at frequencies down to a few terahertz at ambient conditions. The mechanical resonator consists of a collective molecular vibration, which is parametrically coupled to the nanocavity through its Raman polarizability (*23*). This approach allows reaching mechanical frequencies in the 1 to 100 THz range. Our experiment is conceptually presented in Fig. 1, A to D. A dual-band "nanoparticle-in-groove" plasmonic nanocavity (Fig. 1, E and F) is realized by placing a single Au nanoparticle (150 nm nominal diameter) inside a nanogroove etched in a gold film and covered by a monolayer of biphenyl-4-thiol (BPhT) acting as spacer and molecular oscillator (Fig. 1, B and C). Being non-centrosymmetric, BPhT supports vibrational modes that are both IR and Raman active (fig. S13 and supplementary materials, section 1.5), and we used such a mode at 32.4 THz. Our structure is engineered to support colocalized plasmonic resonances at IR and VIS frequencies, which can be excited under normal incidence illumination (fig. S12 and supplementary materials, section 1.4) and correspond to near fields confined in the nanometer-wide gaps formed by the molecular layer (Fig. 1, G to J). The IR resonance frequency is governed by the length of the nanogroove (*30*) (fig. S2), which was chosen as 2 μm to match the vibration frequency of BPhT at $\nu_m \simeq 32.4$ THz.

When a pump laser tuned at 405 THz (740 nm) is focused on the sample (Fig. 2A), the parametric interaction with the molecular vibrations generates Raman sidebands at lower (Stokes) and higher (anti-Stokes) frequencies (Fig. 2B). The giant enhancement factor described

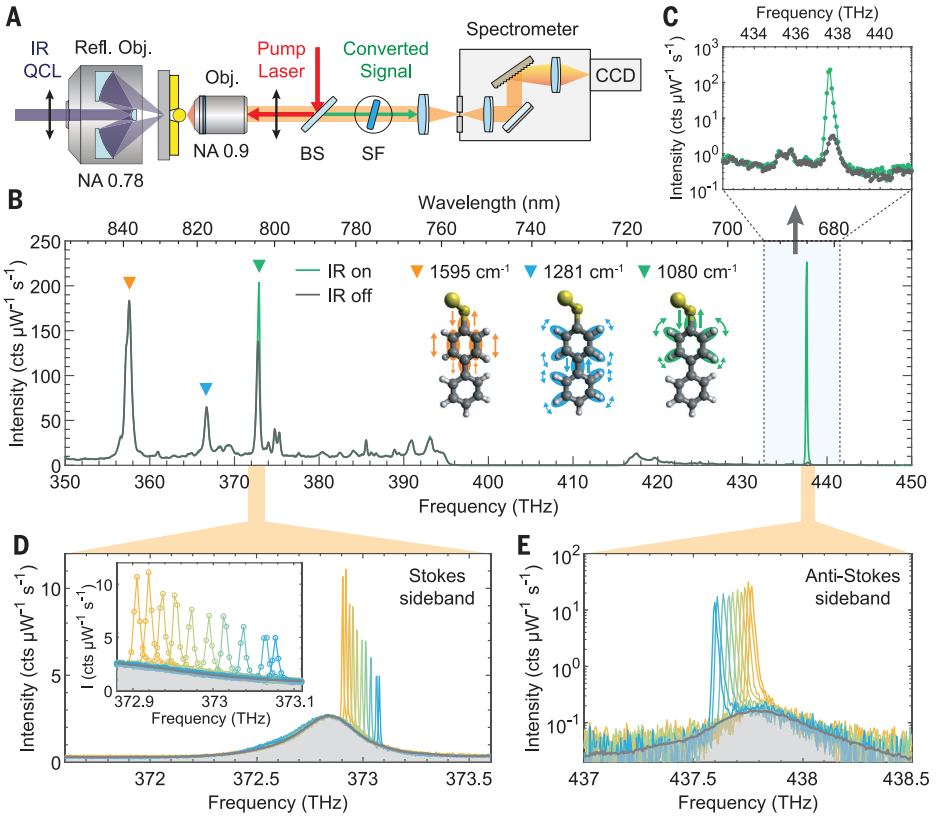

Fig. 2. Molecular optomechanical transduction from 32 THz to the visible domain. (**A**) Schematic of the setup. A reflective objective with numerical aperture (NA) 0.78 focuses the IR beam from a quantum cascade laser (QCL) through the Si substrate while a refractive objective (NA 0.9) focuses the visible pump beam and collects the Raman signal, which is directed to a spectrometer after blocking the pump light with spectral filters (SF). The polarization of pump and IR radiation is perpendicular to the nanogroove (black arrows). BS, beam splitter. (**B**) Low-resolution broadband Raman spectra from a single nanocavity under 10 μW pump power (740 nm wavelength) without (black line) and with (green line) incoming IR radiation (530 μW) near resonant with the BPhT vibration at 32.4 THz (1080 cm^{-1}). The inset shows the vibration patterns of some Raman-active modes labeled with orange, blue, and green triangles. Acquisition time was 10 s. (**C**) Zoom on anti-Stokes sideband plotted on a logarithmic vertical scale. (**D** and **E**) High-resolution (0.23 cm^{-1}, 7 GHz) Stokes (D) and anti-Stokes (E, logarithmic vertical scale) spectra measured when tuning the IR frequency (range limited by the QCL), all normalized to 175 μW of incoming IR power (pump: 10 μW). The gray lines and areas are the spectra without IR radiation and their Lorentzian fits. The inset of (D) shows an enlarged view of the resolution-limited upconverted peak (compare figs. S7 and S8). Acquisition times for the upconverted signals, spontaneous Stokes spectra, and anti-Stokes spectra were 10, 300, and 600 s, respectively.

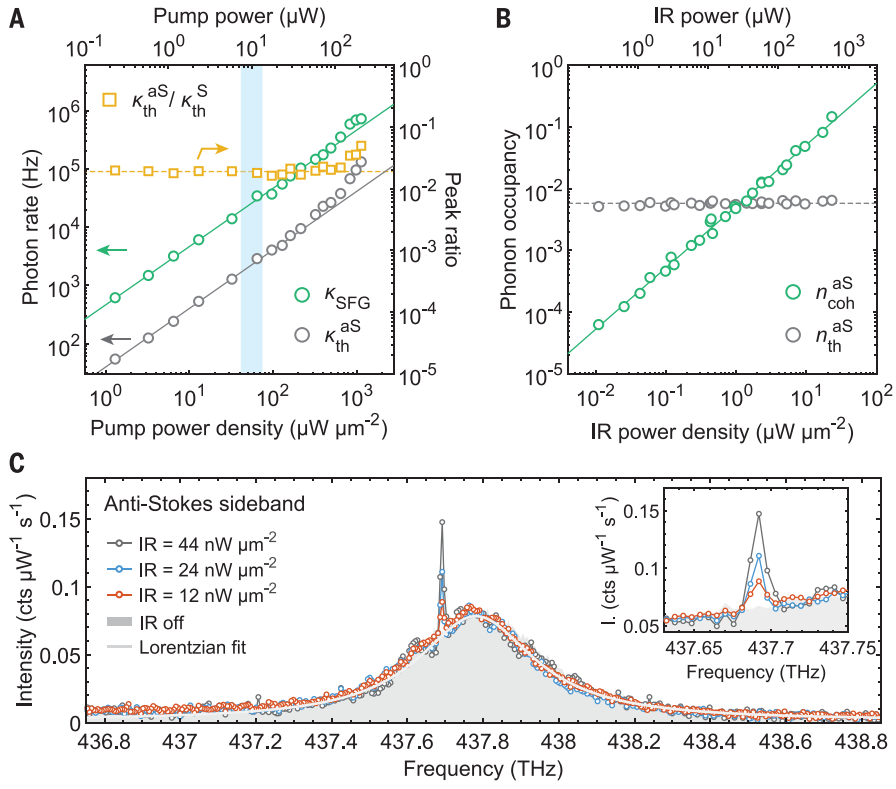

Fig. 3. Dependence of thermal and upconverted signals on IR and VIS powers. (**A**) Gray and green circles represent the rates of thermal (κ_{th}^{aS}) and upconverted (κ_{SFG}; for 600 μW IR power) anti-Stokes photons, respectively, as a function of VIS pump power (tuned at 740 nm). The ratio of thermal anti-Stokes to Stokes signals (without IR input) is plotted as orange squares. Solid lines are linear functions; the dashed line is a constant. The blue shaded area denotes the power range used in other upconversion measurements. (**B**) IR-driven anti-Stokes coherent occupancy n_{coh}^{aS} (green circles) extracted from the sharp peak area [compare with (C)], together with the thermal occupancy inferred from the area of the broad anti-Stokes emission (gray circles) as a function of incident IR power (VIS pump power 10 μW, tuned at 740 nm). The green line is a linear fit; the dashed line is a constant. To convert peak area to phonon occupancy, we assumed that the molecules were at 25°C without IR input. (**C**) Detection of submicrowatt IR signals using high-resolution spectroscopy on the anti-Stokes sideband. Acquisition time was 600 s.

above makes it possible to detect the Raman signal from few hundred molecules, as estimated from the VIS mode area (fig. S12) and molecular layer density (see the supplementary materials, section 1.6). Without IR beam incident on the device (black solid line in Fig. 2B), the Stokes signal is dominated by spontaneous emission of phonon-photon pairs, whereas the anti-Stokes signal originates from the upconversion of thermal vibrations (*31*). At room temperature (T = 25°C), the thermal occupancy of the vibrational mode at ν_m = 32 THz is

$$n_{th} = \left(\exp\left(\frac{h\nu_m}{k_B T}\right) - 1\right)^{-1} \simeq 5.8 \times 10^{-3}$$

where h and k_B are Planck's and Boltzman's constants, respectively.

When the IR beam from a quantum cascade laser was focused through the Si substrate onto the back side of the device (Fig. 2A), we observed two new peaks at the corresponding Raman shift on the Stokes and anti-Stokes sidebands (green line in Fig. 2, B and C), the linewidth of which was much narrower than the natural linewidth of the spontaneous Raman scattering peaks (Fig. 2, D and E). Altogether, these observations are compatible with a coherent upconversion process as pictured in Fig. 1D. As we tuned the frequency of the incoming field, the upconverted signal shifted accordingly, and its measured linewidth was found to be limited by that of our spectrometer, with a value of 7 GHz or 0.23 cm^{-1} (compare fig. S8), which is well below that of single-molecule Raman linewidths typically observed at room temperature (see the supplementary materials, section 2.2). The relative conversion efficiency versus detuning is plotted in fig. S7 and confirms that upconversion is assisted by the vibrational mode.

We interpret these results as being the manifestation of optomechanical transduction, in which a collective molecular vibrational mode is resonantly driven by the nanocavity-enhanced incoming IR field. Because of the ~50 times larger mode volume in the IR versus VIS domain (compare Fig. 1, G to J, and fig. S12), many of the molecules covering the groove may be vibrationally excited yet remain silent in Raman scattering. In the following, we consider only the subset of molecules that are in the region where IR and VIS near fields strongly overlap, which contains a few hundred molecules at most (see calculation in the supplementary materials, section 1.6). We can describe their collective vibrational state by a displaced thermal state with a coherent amplitude α and a corresponding coherent occupancy $n_{coh} = |\alpha|^2$. This coherent, IR-driven oscillation is mapped onto the Raman sidebands of the pump laser, where the IR signal can be analyzed and detected using Si-based detectors. Without IR drive, the Stokes and anti-Stokes photon rates are proportional to $1 + n_{th}$ and n_{th}, respectively; with IR drive, these rates become proportional to $1 + n_{th} + n_{coh}^{S}$ and $n_{th}^{aS} + n_{coh}$, respectively. We added the superscripts "S" and "aS" to highlight that the observed value of n_{coh} depends on the overlap between Raman scattered and IR near fields. Knowing n_{th}, we can extract $n_{coh}^{S,aS}$ from the measured Raman count rate with and without IR drive or, equivalently, from the area subtended by the sharp upconverted peak versus that of the broad spontaneous or thermal emission. Moreover, under the approximation $n_{th} \ll 1$, the Stokes sideband offers a self-calibrated measurement of n_{coh}^{S}. For most nanocavities, we found $0.1 \leq n_{coh}^{S} \leq 0.5$ for 500 to 600 μW IR power (compare table S2), corresponding to 20 to 24 μW/μm^2 IR power density at the spot's center (fig. S17). This figure is compatible with an enhancement of IR absorption cross section per molecule by more than five orders of magnitude, as predicted from field enhancement simulations and detailed in the supplementary materials, section 1.6.

When varying the power of the pump laser at 740 nm, we observed a linear dependence of the upconverted Raman signal from 0.1 to 100 μW (green circles in Fig. 3A), which is consistent with the expected parametric upconversion process. In this power range, the spontaneous Stokes and thermal anti-Stokes signals also grow linearly with pump power, and their ratio remains constant (gray circles and yellow squares in Fig. 3A; see also fig. S10). An optomechanical description of plasmon-enhanced Raman scattering (*8*, *23*, *32*) predicts three main regimes for the pump power dependence of the spontaneous Stokes and anti-Stokes signals: (i) at low power, a linear regime dominated by thermal noise;

then (ii) a quadratic increase of anti-Stokes intensity as the vibrational population increases linearly with laser power due to quantum back action, yet remains small against unity (also called vibrational pumping) (*24*, *26*, *33*); and finally (iii) a phonon-stimulated regime is expected, dominated by dynamical back-action amplification of the vibration (*23*), where both Stokes and anti-Stokes powers diverge and the harmonic potential approximation breaks down. The data in Fig. 3A are compatible with regime (i) except >100 μW, where signatures of regime (ii) may be inferred; however, the behavior is not always reversible at such powers, suggesting that permanent changes in the nanocavity affected the observations. Figure 3B shows that the upconverted anti-Stokes signal scales linearly with incoming mid-IR power, as expected for a resonant drive well below saturation. We also plotted with gray circles the area of the thermal incoherent anti-Stokes peak, which shows a slight increase with IR power. As detailed in fig. S16, we deduced that the effective temperature of the molecules did not rise by >10°C for the highest IR powers.

Finally, we quantified the external IR to visible conversion efficiency of our device by spectrally filtering the anti-Stokes sideband and sending it to a single-photon-counting module with independently calibrated detection efficiency (results are summarized in table S2). We inferred that the upconverted anti-Stokes photon rate collected by the objective reaches up to 200 kHz per nanocavity for 600 μW incident IR power (corresponding to $n_{IR} \simeq 2.8 \times 10^{16}$ photons/s) at 10 μW pump power. Direct comparison of these incoming and upconverted fluxes yields a conversion efficiency from incoming IR photon to outgoing visible photon collected by our objective on the order of 10^{-12} (fig. S5), or 10^{-7}/W of pump power. Only 6% of the power emitted in the near field was collected by our objective, as simulated in Fig. S12E, so that the internal efficiency is at least 15 times larger. Despite the low efficiency, the coherent nature of the process allowed us to reliably detect incoming IR powers densities down to tens of nanowatts per square micrometer, as shown in Fig. 3C, a figure that would further improve with the increasing resolution of the spectrometer.

We present an optomechanical nanocavity leveraging molecular vibrations that are both IR and Raman active for coherent frequency conversion between the mid-infrared and visible domains. Subwavelength device dimensions elude the need for phase matching and permit the extension of spectral coverage by the mere choice of molecule (*34*) (figs. S14 and S15) and adjustment of plasmonic resonance (fig. S2). We identified several parameters that can be improved to increase conversion efficiency, notably a better overlap between IR and VIS near fields, a larger number of nanocavity-coupled molecules, and a higher resilience to Raman pump power. Operating our device in the vibrational strong coupling regime may enable efficient bidirectional IR ↔ VIS operation (see the supplementary materials, section 2.1). Finally, our concept is compatible with photonic integrated circuits and with the realization of chip-scale pixel arrays used as IR spectrometers and hyperspectral imagers.

Note added in proof: Related experiments are independently reported (*35*).

REFERENCES AND NOTES

1. S. De Bruyne, M. M. Speeckaert, J. R. Delanghe, *Crit. Rev. Clin. Lab. Sci.* **55**, 1–20 (2018).
2. F. Ciampa, P. Mahmoodi, F. Pinto, M. Meo, *Sensors* **18**, 609 (2018).
3. T. L. Roellig *et al.*, *J. Astron. Telesc. Instrum. Syst.* **6**, 041503 (2020).
4. A. Rogalski, *Infrared and Terahertz Detectors* (CRC Press, ed. 3, 2019).
5. D. A. Kalashnikov, A. V. Paterova, S. P. Kulik, L. A. Krivitsky, *Nat. Photonics* **10**, 98–101 (2016).
6. C. Lindner *et al.*, *Opt. Express* **29**, 4035–4047 (2021).
7. A. Barh, P. J. Rodrigo, L. Meng, C. Pedersen, P. Tidemand-Lichtenberg, *Adv. Opt. Photonics* **11**, 952–1019 (2019).
8. P. Roelli, D. Martin-Cano, T. J. Kippenberg, C. Galland, *Phys. Rev. X* **10**, 031057 (2020).
9. N. Lauk *et al.*, *Quantum Sci. Technol.* **5**, 020501 (2020).
10. N. J. Lambert, A. Rueda, F. Sedlmeir, H. G. L. Schwefel, *Advanced Quantum Technologies* **3**, 1900077 (2020).
11. G. Temporão *et al.*, *Opt. Lett.* **31**, 1094–1096 (2006).
12. Y.-P. Tseng, C. Pedersen, P. Tidemand-Lichtenberg, *Opt. Mater. Express* **8**, 1313–1321 (2018).
13. S. Roke, G. Gonella, *Annu. Rev. Phys. Chem.* **63**, 353–378 (2012).
14. C. S. Tian, Y. R. Shen, *Surf. Sci. Rep.* **69**, 105–131 (2014).
15. Y. Chu, S. Gröblacher, *Appl. Phys. Lett.* **117**, 150503 (2020).
16. T. Bagci *et al.*, *Nature* **507**, 81–85 (2014).
17. R. W. Andrews *et al.*, *Nat. Phys.* **10**, 321–326 (2014).
18. A. Vainsencher, K. J. Satzinger, G. A. Peairs, A. N. Cleland, *Appl. Phys. Lett.* **109**, 033107 (2016).
19. K. C. Balram, M. I. Davanço, J. D. Song, K. Srinivasan, *Nat. Photonics* **10**, 346–352 (2016).
20. M. Forsch *et al.*, *Nat. Phys.* **16**, 69–74 (2020).
21. M. Mirhosseini, A. Sipahigil, M. Kalaee, O. Painter, *Nature* **588**, 599–603 (2020).
22. C. Belacel *et al.*, *Nat. Commun.* **8**, 1578 (2017).
23. P. Roelli, C. Galland, N. Piro, T. J. Kippenberg, *Nat. Nanotechnol.* **11**, 164–169 (2016).
24. M. K. Schmidt, R. Esteban, F. Benz, J. J. Baumberg, J. Aizpurua, *Faraday Discuss.* **205**, 31–65 (2017).
25. S. Tarrago Velez, V. Sudhir, N. Sangouard, C. Galland, *Sci. Adv.* **6**, eabb0260 (2020).
26. F. Benz *et al.*, *Science* **354**, 726–729 (2016).
27. M. P. Nielsen, X. Shi, P. Dichtl, S. A. Maier, R. F. Oulton, *Science* **358**, 1179–1181 (2017).
28. S. Ummethala *et al.*, *Nat. Photonics* **13**, 519–524 (2019).
29. Y. Salamin *et al.*, *Nat. Commun.* **10**, 5550 (2019).
30. C. Huck *et al.*, *ACS Photonics* **2**, 1489–1497 (2015).
31. S. T. Velez *et al.*, *Phys. Rev. X* **9**, 041007 (2019).
32. M. K. Schmidt, R. Esteban, A. González-Tudela, G. Giedke, J. Aizpurua, *ACS Nano* **10**, 6291–6298 (2016).
33. K. Kneipp *et al.*, *Phys. Rev. Lett.* **76**, 2444–2447 (1996).
34. Z. Koczor-Benda, P. Roelli, C. Galland, E. Rosta, "Molecular vibration explorer" (Materials Cloud, 2021); https://molecular-vibration-explorer.matcloud.xyz/voila/render/index.ipynb.
35. A. Xomalis *et al.*, *Science* **374**, 1268–1271 (2021).
36. Data for: W. Chen *et al.*, Continuous-wave frequency upconversion with a molecular optomechanical nanocavity, Zenodo (2021); https://doi.org/10.5281/zenodo.5558767.

ACKNOWLEDGMENTS

C.G. is indebted to V. Sudhir for valuable comments and fruitful discussions about the results. W.C. and C.G. thank H. Altug for providing access to an FTIR spectrometer and acknowledge support from the IPHYS mechanical workshop, characterization platform, and EPFL CMi cleanroom. **Funding:** This work received funding from the European Union's Horizon 2020 Research and Innovation Program under grant agreement nos. 829067 (FET Open THOR), 820196 (ERC CoG QTONE), and 732894 (HOT). C.G. acknowledges support from the Swiss National Science Foundation (project nos. 170684 and 198898). This work is part of the research program of the Netherlands Organisation for Scientific Research (NWO). A.I.B. acknowledges financial support by the Alexander von Humboldt Foundation. **Author contributions:** W.C. designed and fabricated the devices, performed the experiments, analyzed the data, and created the main figures. P.R. performed calculations of molecular parameters, assisted in the early stages of the experiments, and assisted in data analysis. H.H. performed the electromagnetic simulations of nanocavities and contributed to nanocavity design. S.V. assisted in recording and analyzing the photon-counting data. S.P.A. contributed to setting up the experimental apparatus. A.I.B., M.K., and A.M. conceived and fabricated the first generation of nanogroove cavities. T.J.K. contributed to early ideas leading to this work and commented on the manuscript. E.V. and A.M. discussed the results and contributed to writing and improving the manuscript. C.G. designed and supervised the study, analyzed the data, and wrote the manuscript with the assistance of W.C., P.R., H.H., E.V., and A.M. **Competing interests:** The authors declare no competing interests. **Data and materials availability:** All data supporting this report are available in the Zenodo repository (*36*).

SUPPLEMENTARY MATERIALS

science.org/doi/10.1126/science.abk3106
Materials and Methods
Supplementary Text
Figs. S1 to S17
Tables S1 and S2
References (*37*–*79*)

6 July 2021; accepted 12 October 2021
10.1126/science.abk3106

Science

Continuous-wave frequency upconversion with a molecular optomechanical nanocavity

Wen ChenPhilippe RoelliHuatian HuSachin VerlekarSakthi Priya AmirtharajAngela I. BarredaTobias J. KippenbergMiroslavna KovylinaEwold VerhagenAlejandro MartínezChristophe Galland

Science, 374 (6572), • DOI: 10.1126/science.abk3106

Optomechanical upconversion

Molecules have rich signatures in their spectra at infrared wavelengths and are typically accessed with dedicated spectroscopic instrumentation. Chen *et al*. and Xomalis *et al*. report optomechanical frequency upconversion from the mid-infrared to the visible domain using molecular vibrations coupled to a plasmonic nanocavity at ambient conditions (see the Perspective by Gordon). Using different nanoantenna designs, one with a nanoparticle-on-resonator and the other with nanoparticle-in-groove, both approaches show the ability to upconvert the mid-infrared vibrations of the molecules in the nanocavity to visible light wavelengths. The effect could be used to simplify infrared spectroscopy, possibly with single-molecule sensitivity. —ISO